Adhesion, Friction, and Mechanical Properties of Functionalized Alkanethiol Self-Assembled Monolayers

JACK E. HOUSTON*,† AND HYUN I. KIM‡
Sandia National Laboratories, Albuquerque, New Mexico 87185-1415, and Aerospace Corporation, Los Angeles, California 90009-2957

Received December 3, 2001

ABSTRACT
We have used interfacial force microscopy to study the adhesion, friction, and mechanical properties of molecular monolayers self-assembled on Au surfaces. This quantitative and stable scanning-probe technique permits detailed studies of these factors. By systematic variation of the chemical nature of the end groups on the monolayers and utilization of standard and intuitive contact-mechanics models, quantitative results are presented of inter- and intrafilm bonding strength as well as the relationship between mechanical behavior and the lateral friction force.

Introduction

Considerable interest has recently been generated in the potential use of self-assembled monolayer (SAM) films as lubricants for such applications as micro-electromechanical machines (MEMS).[1] In addition, broad discussions have appeared in the literature addressing the details of friction at the molecular level, especially with regard to determining the relationship between adhesion and friction.[2] Extensive experimental work has already been done in these areas using the surface forces apparatus[3−6] and the atomic force microscope,[7,8] and recent reviews of the general area have appeared.[9] However, both of these instruments measure force using deflection sensors, i.e., where a spring element deflects under the force and the force value is measured by the degree of deflection. Such sensors suffer from a mechanical instability that exists when the gradient of the interfacial force equals the spring constant of the elastic element, giving rise to the so-called "jump-to-contact" instability.[10] In fact, this instability is so common in interfacial force measurements that the strength of interfacial adhesion is usually characterized in terms of a single parameter called the "pull-off force", i.e., the force at the point of the pull-off instability.[11] Thus, the relationship between normal force and friction is not available over a considerable range of the attractive regime. In addition, the adhesive strength is defined by the work done in breaking the adhesive bond and requires a measurement of the integral of the normal force as a function of displacement as the two surfaces are separated. However, the pull-off-force only measures the maximum value of the adhesive force and misses the important role of the mechanical aspects of the adhesive strength. This role affects adhesive strength in practical areas ranging from commercial adhesives to molecular interactions mediated by protein folding. For example, good adhesives are normally polymers because they plastically deform during bond stress. The energy lost in the plastic process dramatically increases the work necessary to cause bond failure.

The interfacial force microscope (IFM) solves the problem of the sensor instability by operating with a self-balancing, force-feedback sensor, which provides quantitative and stable force measurements over the entire range of interfacial interaction—including the attractive region.[12] This capability allows the technique to produce unique results relating to measurements of the relationship among interfacial bonding, friction, and mechanical properties. Specifically, we report here the use of the IFM to study the mechanical and chemical mechanisms that govern friction forces for alkanethiol SAM films grown on Au surfaces. The major focus is on the simultaneous measurement of the normal force (both attractive and repulsive) and the lateral friction force for SAM-coated probe and sample surfaces. The chemical nature of the SAM surfaces is systematically varied by using combinations of end groups with distinct functionality, while the mechanical properties are altered by using films of differing alkyl chain lengths. We then use a popular and intuitive model for the contact mechanics to arrive at quantitative values for the composite modulus, the energy of adhesion, and the friction shear strength for the interfacial interactions.

Self-Balancing, Force Feedback IFM Sensor

The IFM sensor consists of a capacitor common plate suspended above two individual capacitor pads by torsion bars bisecting the long axis, as illustrated schematically in Figure 1. A tip is placed on one side of this "teeter totter" such that when a force is applied to the tip, arising from the interaction with a neighboring sample surface, the teeter totter will rotate about the torsion bars imbalancing the differential capacitance. The deflection is measured by an RF bridge circuit, and the resulting signal is fed to a controller which applies the appropriate dc voltages to the capacitor pads to rebalance the deflection. The result is that voltages appear at the controller output related to the level of applied force without sensor motion. The relationship between the voltage and force is depend-

Jack E. Houston received his Ph.D. in physics in 1965 from Oklahoma State University. He is presently a Distinguished Member of the Technical Staff at Sandia National Laboratories in Albuquerque, NM. His interests include the application of scanning-probe techniques to the study of the physics and chemistry of surfaces and interfaces.

Hyun I. Kim received his Ph.D. in chemistry from University of Houston in 1999. This was followed by a two year postdoctoral appointment at Sandia National Laboratories in Albuquerque, NM. He then joined Aerospace Corp. in El Segundo, CA, as a Member of the Technical Staff. His interests include the control and characterization of surface and interfacial properties using scanning probe microscopy and other surface science techniques.

† Sandia National Laboratories.
‡ Aerospace Corp.

10.1021/ar9801144 CCC: $22.00
Published on Web 05/22/2002

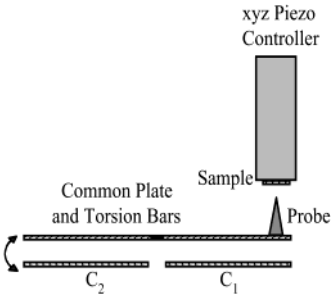

FIGURE 1. Schematic of the differential-capacitor IFM force-feedback sensor. The common plate supports the probe tip and is suspended above two capacitor pads by torsion bars going in and out of the page. Interactions between the tip and sample rotate the top plate, which is detected by an rf bridge. Low-frequency voltages are then supplied to the capacitor pads by a controller to maintain capacitor balance.

ent only on the capacitor geometry and is easily calibrated. In addition, the force-feedback sensor will balance any force applied to the tip which produces a torque about the torsion-bar axis, and it is this fact that is the basis for making lateral-force measurements in the friction mode, as described below.

Friction forces are measured by two methods. The first utilizes a constant-torque mode by displacing the sensor and probe assembly laterally along a direction perpendicular to the torsion-bar axis and monitoring changes in the relative tip/sample separation to maintain a constant level of torque.[13,14] If the tip displacement is away from the torsion-bar axis, the sensor detects an increase in torque and moves back to maintain the torque. Lateral displacement in the opposite direction will result in a tip displacement toward the sample to compensate for the decrease in torque. Thus, if the assembly is scanned first in one direction and then back in the other, the piezo deflection will form a displacement loop or "friction loop" similar to those commonly observed in the atomic force microscope friction mode.[15] To relate the size of the displacement loop to the friction force, one needs to know the relationship between displacement and force resulting from the tip/sample contact, which is characterized by performing nanoindentation in sequence with displacement-loop measurements to obtain this relationship.[13] Wear measurements are simply done by repeated constant-torque line scans keeping track of the loop areas. In the second method, since the sensor actually balances the torque applied to the tip, normal and lateral forces are simultaneously obtained by placing a small lateral modulation (25 Å at 100 Hz for this work) on the tip and separating the force signals in the frequency domain.[16]

Preparation of the Tip and Substrate Molecular Films

The IFM investigations are done on systems consisting of parabolic gold or tungsten tips (radius and shape determined by SEM) and single-crystal gold surfaces that are modified with SAM films with either $-CH_3$ or $-COOH$ end groups. It is well-known that surface roughness has a dramatic affect on friction. Here, the Au substrates are

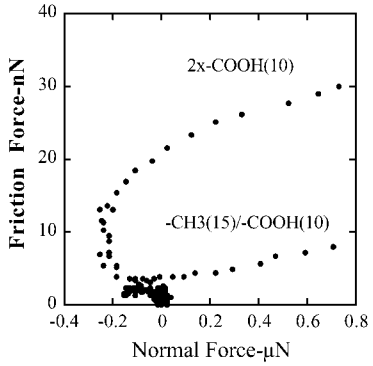

FIGURE 2. Friction force vs normal force for the interaction of a 5000 Å Au tip and single-crystal Au(111) sample functionalized by 2×−COOH(10) and −CH3(15)/−COOH(10) end-group combinations.

atomically flat and the tips are smooth but undoubtedly have atomic level roughness. However, our measurements are all relative using the same substrate and tip. Therefore, the overall conclusions should be relatively unaffected by the slight remaining roughness. The −COOH-terminated films are generated from 1 mM ethanolic solutions (all solutions use the same ethanolic concentration) of either 16-mercaptohexadecanoic acid ($HS(CH_2)_{15}COOH$) or 11-mercaptoundecanoic acid ($HS(CH_2)_{10}COOH$) solutions. The $-CH_3$-terminated films use a *n*-hexadecanethiol ($HS(CH_2)_{15}CH_3$) solution. In the following, we will refer to these according to the number of methylene ($-CH_2$) units as −COOH(15), −COOH(10), and −CH3(15), respectively. The same 5000 Å radius Au tip was used for all combinations. The W tip radius used for the high-force measurements was ∼2000 Å.

Chemical and Mechanical Origins of Molecular-Level Friction

We begin by discussing results aimed at answering a fundamental question relating to the origin of molecular friction; i.e., what are the roles of mechanical disturbance and chemical adhesion in determining the friction force? Here, a Au tip and single-crystal Au substrate are both coated by SAM films terminated by either $-CH_3$ or −COOH end groups. For interactions involving the first, only weak van der Waals forces are expected and the friction should be only due to the mechanical disturbance of the film structure under lateral tip motion, while a symmetric combination of the second can involve significant hydrogen bonding.[17] Figure 2 shows the results for combinations of −CH3(15)/−COOH(10) and 2×−COOH-(10). We will designate the symmetric end-group combinations by, for example, 2×−CH3(15) or 2×−COOH(10). The accumulation of data points near and just below the zero of normal force (negative normal-force values indicate attractive forces) means that the friction force does not begin to rise until contact between the two films, but in all cases this rise begins in the attractive region. As expected, small adhesive interactions and friction forces are seen for the CH3(15)/−COOH(10) combination. Since no chemical interaction (above a weak van der Waals

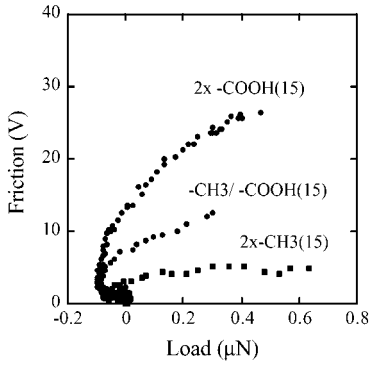

FIGURE 3. Friction force vs normal force for the interaction of 2×−COOH(15), −CH3(15)/−COOH(15), and 2×−CH3(15) end-group combinations.

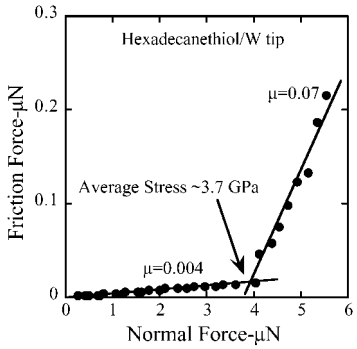

FIGURE 4. Friction force vs normal force for a hexadecanethiol SAM on a Au(111) surface and a bare W tip taken by the friction-loop method. The calculated average applied stress at the break point is 3.7 GPa.

attraction) is seen or expected, the friction results can be attributed entirely to a *mechanical* film disturbance.

In contrast, the data for 2×−COOH(10) in Figure 2 show large adhesion and large friction. The increased friction force results from the breaking of hydrogen bonds as the tip is lateral displaced along the surface. Both the mechanical and bond-breaking processes result in a loss of energy, which winds up principally in molecular vibrations. The shape of the friction vs normal-force curves in Figure 2 is reminiscent of the results obtained earlier on mica surfaces where the shape was interpreted as due to changes in the contact area as the load increases[18]—more about this later.

"Odd/Even" Effect on Friction and Bonding

There is an interesting twist on these results, however. If the number of methylene units in the alkyl backbone is changed from even to odd, the orientation of the −COOH group is altered. In fact, IR data suggest that this change can result in films with considerably different levels of intra- versus interfilm bonding.[19,20] This possibility is tested here by adding to the data of Figure 2 all of the "odd" combinations including −COOH(15), and these results are shown in Figure 3. Now, both the −CH3(15)/−COOH(15) and 2×−COOH(15) show high friction-force behavior but only van der Waals adhesive forces. This result indicates that significant intrafilm hydrogen bonding exists along the surface of the −COOH(15) terminated films and these bonds are also being disturbed by the lateral tip motion.[17]

For these thin lubricating films, the friction vs normal force curves appear to be approaching a linear behavior at the higher levels of normal force. In fact, this was shown to be the case in earlier measurements of friction for alkanethiol SAMs on Au single-crystal surfaces using a parabolic W tip. The friction-loop method was used to be able to obtained friction data at high levels of normal force.[13] Results for a hexadecanethiol film on a Au single-crystal substrate are shown in Figure 4 for normal forces up to ~6 μN. The curve is linear allowing a friction coefficient to be defined, which turns out to be 0.004—a very low value. This value is maintained up to force levels of ~4 μN, after which it suddenly increases to 0.07. Even at the higher forces, however, the coefficient does not increase after wear-track repetitions of several hundred cycles, indicating that such films are very good lubricants with very high breakdown strengths.[13] The normal force at which the sudden slope change occurs corresponds to a calculated average applied stress of ~3.7 GPa. Such a break in friction coefficient indicates that some other energy-loss mechanism has suddenly turned on.

Quantitative Analysis of Low-Load Friction

To more fully exploit the quantitative results of Figures 2 and 3, we use an analysis similar to that applied earlier.[21] Using the Johnson−Kendall−Roberts (JKR) model[22] for the variation of contact area with load, these authors were able to obtain a value for the friction shear strength τ of the interfacial interaction. The friction, or shear force, is then given by the product of τ and the contact area A. The equation describing the friction force vs the normal force is given as[21]

$$F_\mu = (1 + \sqrt{1 + L})^{4/3} \tag{1}$$

where the friction and normal forces F_μ and L have been normalized by their critical values defined by the relationships

$$F_\mu = \frac{F}{F_c} \qquad L = \frac{f}{|f_c|} \tag{2}$$

The critical values F_c and f_c represent the friction and normal-force values at the maximum in the attractive force (commonly called the "pull-off force") and are, in turn, defined by the relationships

$$F_c = \tau A_c = \pi\pi\left(\frac{3\pi\gamma_{12}R^2}{2E^*}\right)^{2/3} \qquad f_c = -\frac{3}{2}\pi R\gamma_{12} \tag{3}$$

where A_c is the critical contact area (the area at the maximum attractive force), R is the tip radius, and γ_{12} is the energy of adhesion (corresponding to the work/unit area required to separate the surfaces). The subscript indicates a general form where the two interacting surface are different. In the case where they are the same, $\gamma_{12} = 2\gamma$, where γ is the surface energy of the two interacting

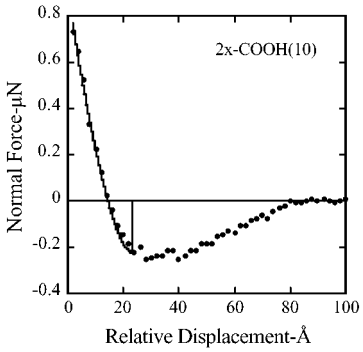

FIGURE 5. Normal force vs relative tip displacement for the 2×−COOH(10) interaction (closed circles). The solid curve indicates the JKR fit to the force profile. Similar levels of fitting are obtained for all the combinations and yield parameters summarized in Table 1.

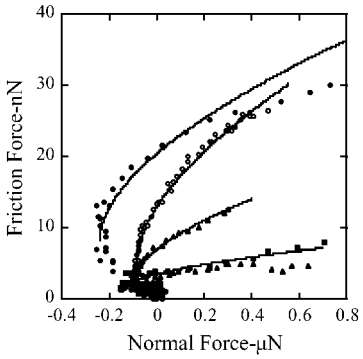

FIGURE 6. Friction force vs normal force for the interaction of the combinations: filled circles, 2×−COOH(10); open circles, 2×−COOH-(15); filled triangles, −CH3(15)/−COOH(15); open diamonds, 2×−CH3-(15). The solid curves represent the JKR fits to the respective combinations with the resulting parameters tabulated in Table 1.

surfaces. E^* is the reduced modulus given by the expression

$$\frac{1}{E^*} = \frac{1-\nu_t^2}{E_t} = \frac{1-\nu_s^2}{E_s} \tag{4}$$

where E_t, E_s, ν_t, and ν_s are the modulus and Poisson-ratio values for the tip and sample materials.

The analysis of the data to obtain a value for the friction shear strength τ requires a knowledge of three unknowns (eq 3), i.e., the tip radius R (5000 Å in this case), the energy of adhesive γ_{12}, and the composite modulus E^*. Both γ_{12} and E^* values are obtained from a JKR analysis[22] of the normal force vs relative displacement data, an example of which is shown as the dotted curve in Figure 5 for the 2×−COOH(10) interaction. The JKR analysis further requires a knowledge of the contact radius a and the film deformation δ. The contact radius is given by an equation similar to eq 1; i.e.,

$$a = \left(\frac{R|f_c|}{E^*}\right)^{1/3}(1+\sqrt{1+L})^{2/3} \tag{5}$$

and the relationship between δ and a takes the form

$$\delta = \frac{a^2}{R}\left[1 - \frac{2}{3}\left(\frac{a_c}{a}\right)^{3/2}\right] \tag{6}$$

where a_c is the value of a at the point of maximum adhesive force.

The advantage of obtaining the value of E^* in this way is that the modulus and Poisson's ratio values necessary to calculate E^* from eq 4 are not known for these very thin films. In addition, the E^* value is a combination of the parameters for the two films as well as the substrate and tip. All of these factors are taken into account by obtaining the E^* value from experiment. The JKR fit resulting from this analysis is shown as the solid curve in Figure 5. (Note that, because only contact forces are considered in this model, the calculated force is zero until contact is made, after which it suddenly jumps to its maximum attractive value.) The resulting parameters are tabulated, along with those obtained from data similar to that of Figure 5 for the other end-group combinations, in Table 1. With the γ_{12} and E^* values determined through this procedure, we are in a position to use eqs 1−3 to fit the friction vs normal force data and obtain the value for the friction shear strength τ. The result of this analysis for the data of Figures 2 and 3 is shown in Figure 6 (except for the 2×−CH3(15) case, which is very similar to that obtained for −CH3(15)/−COOH(10)) and compiled in Table 1.

Table 1. Parameters from a Johnson−Kendall−Roberts[22] Analysis of the Data of Figures 2 and 3

end groups	E^* (Gpa)	γ_{12} (mJ/m^2)	τ (Mpa)	$(CH_2)_{n1+n2}$
2×−COOH(10)	16	93	6.5	20
2×−COOH(15)	4	42	3.2	30
−CH3(15)/−COOH(15)	4	42	1.6	30
−CH3(15)/−COOH(10)	10	42	1.5	25
2×−CH3(15)	5	37	0.8	30

The role of the Au tip and substrate compliance is clearly evident in the tabulated values of E^*. The shortest molecular combination, i.e., 2×−COOH(10) with a total of 20 CH_2 units (shown as the last column in Table 1), i.e., $(CH_2)_n$ with $n = 20$, shows the highest E^* value followed by −CH3(15)/−COOH(10) with 25 units. The other combinations have 29 or 30 units and the lowest E^* values. The SAM film becomes trapped between the Au tip and substrate, which both have a modulus of 78 GPa.[23] Until the film is dramatically strained, the two materials appear as two springs in series, where the total deformation is the sum of that due to the film and the tip/substrate combination, while the force is the same on both materials. With greater strain, the films become virtually noncompliant and the deformation is eventually due entirely to the Au compliance. In fact, this behavior has been used in nanoindentation experiments to study the fundamental properties of a Au single-crystal surface in the absence of tip/substrate adhesion.[24−27] The compliance behavior of these short-chain molecules is highly nonlinear, and it is somewhat fortuitous that they produce a reasonable fit to the simple contact-mechanics models, but this fitting works only over a small range of repulsive force. Lacking detailed calculations, this simple characterization is the only reasonable path available to quantify the frictional parameters.

We see from Table 1 that, as expected, 2×−COOH(10) has the highest adhesive strength, greater by more than a factor of 2 than all the other combinations. For the combinations involving −CH3(15), we see that the E^* and γ_{12} values are consistent with the total film lengths and the hydrophobic nature of the −CH3-terminated surface. The fact that the 2×−COOH(15) and −CH3(15)/−COOH-(15) combinations have the same low value of γ_{12} indicates that the −COOH(15) surface is virtually hydrophobic. The surface energy γ for the symmetric combinations is just half the γ_{12} values from Table 1. For 2×−COOH(10), this value would be about ∼46 mJ/m^2, while the 2×−COOH-(15) and 2×−CH3(15) have values of approximately 20 mJ/m^2. The former is about 65% of the 73 mJ/m^2 measured for water,[11] and the latter two are somewhat less than the ∼27 mJ/m^2 found for *n*-hexadecane liquid.[11] Here again, this latter value emphasizes the level of hydrophobicity of the −COOH(15) surface, which is only slightly greater than that obtained from the very hydrophobic 2×−CH3-(15) interaction.

If we assume that the mechanical and adhesive aspects of friction are the same, the shear-strength values from Table 1 suggest that the level of interfilm bonding involved in the 2×−COOH(10) interaction is virtually double that of the intrafilm bonding for the 2×−COOH(15) interaction. However, a similar comparison between the shear-strength values for 2×−CH3(15) and −CH3(15)/−COOH-(10) indicates that this assumption is not justified. Similar to the E^* results, the higher τ value for the shorter combination indicates that the mechanical disturbance of the shorter-length films is greater. Several authors have found this to be the case.[28−30] At this point it is not possible to accurately evaluate the relationship between chain length and τ. This would require a broader range of combinations, for example, measurements of combinations involving −CH3-terminated SAM films of various lengths.

If we may be permitted to skirt the realm of pure speculation, we could assume that the mechanical and adhesive contributions to the friction for the various interaction combinations are additive. Thus, taking 2×−CH3(15) to represent a purely mechanical interaction, we will take the mechanical contribution for a single layer of long molecules to be half the τ value of Table 1, or approximately 0.4. Then from the long/short combination [−CH3(15)/−COOH(10)], which according to the γ_{12} value is purely mechanical, we deduce that the mechanical contribution for a single layer of short molecules is 1.1 (1.5 − 0.4). By subtracting these mechanical contributions from the total τ's for the other combinations, we find the separate values for the mechanical and bonding contributions summarized in Table 2. These turn out to be negligible for those films involving −CH3(15) and −COOH-(10) molecules, as expected. The large difference between the values for 2×−COOH(10) and 2×−COOH(15) would imply that the bonding strength/unit area is greater for the "adhesive" interaction of the former than for the "cohesive" interaction of the latter. This would seem to be plausible considering the steric flexibility of the molecules meeting head on, where the end groups can maximize their interfilm bonding, compared with interactions between the end groups of neighboring molecules leaning ∼30° from the normal in the SAM packing arrangement. The factor of 3 in the τ-bonding values between 2×−COOH(15) and −CH3(15)/−COOH(15) is less obvious. Since, nominally, there would be twice as many intrafilm bonds for two interacting −COOH(15) films than for just one, we would expect a factor of 2 between the τ-bonding values. However, as we pointed out above, the differing τ-bonding values for 2×−COOH(15) and 2×−COOH−OH(10) indicate that unsatisfied bonds remain on the 2×−COOH(15) film and these may be available for *interfilm* bonding, giving rise to increased friction. The answer as to whether this is the case, or whether the discrepancy reflects the crude approximation used to calculate these values, will have to await further, more careful measurements which include a wider variety of combinations of both end-group functionality and molecular length.

Table 2. Bonding Portion of the Friction Shear Strength under the Assumption That the Mechanical and Bonding Portions Are Simply Additive[a]

	τ (MPa)		
end groups	tot.	mechanical	bonding
2×−COOH(10)	6.5	2.2	4.3
2×−COOH(15)	3.2	0.8	2.4
−CH3(15)/−COOH(15)	1.6	0.8	0.8
−CH3(15)/−COOH(10)	1.5	1.1	0.4
2×−CH3(15)	0.8	0.8	0.0

[a] The first column is from Table 1 followed by values for the τ-mechanical and τ-bonding portions of the measured shear strength.

Friction and Mechanical Properties at Higher Loads

At normal forces in excess of about 1 μN (for our 5000 Å tip radius) the film becomes quite nonlinear and eventually noncompliant. We can illustrate this behavior from data taken in conjunction with earlier work aimed at obtaining the role of stress in the conductance behavior of hexadecanthiol films probed by a 2000 Å W tip.[31] The force profile for this system is shown as open circles in Figure 7 along with the JKR fit shown as a solid line. The fit was done with a γ_{12} value of approximately zero and the handbook values for the modulus and Poisson ratios for Au and W, i.e., E values of 78 and 411 GPa and ν values of 0.44 and 0.28, respectively.[23] The resulting E^* value (from eq 4) for this combination is 83 GPa. As one can see from Figure 7, the fit is very good except for the low- and high-force regions. These are the regions where the film compliance is significant, whereas the regions of close fit signal very small film compliance. As mentioned earlier, we can calculate the film compliance by assuming that the problem can be viewed as two springs in series. Under this assumption, the deformation of the film can be calculated from the expression

$$d' = d + \left(F/\frac{4}{3}\sqrt{R}E^*\right)^{2/3} \qquad (7)$$

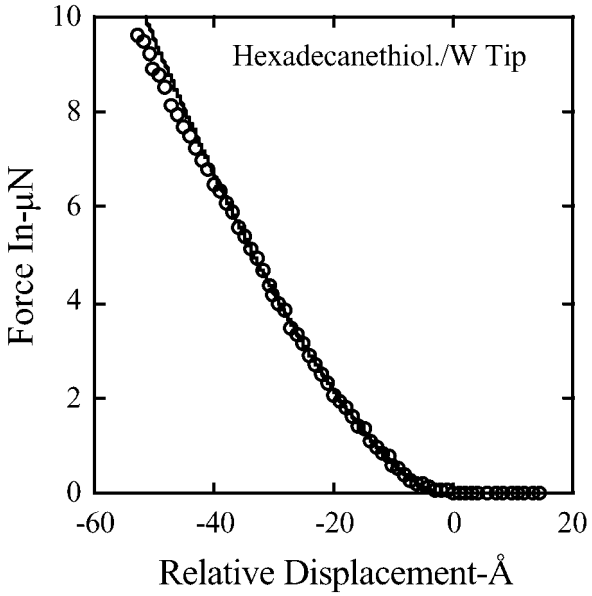

FIGURE 7. Normal force vs relative tip displacement for a hexadecane SAM on a Au(111) surface and a bare 2000 Å W tip. The solid line represents the JKR fit and shows significant film compliance at both low and high values of normal force.

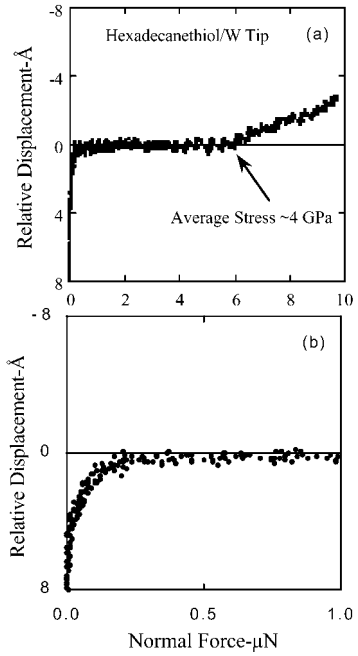

FIGURE 8. (a) Compliance of a hexadecanethiol SAM film on a Au(111) surface probed by a 2000 Å W tip resulting from the removal of the tip/sample compliance through the use of eq 7. (b) An expanded view of the high-compliance region in (a).

where d' is the film deformation, d is the total (measured) deformation, F is the normal force, and R and E^* are defined as before. Applying this equation to the data of Figure 7 results in the film compliance behavior shown in Figure 8. Figure 8b shows an expanded view of the low-force region of Figure 8a. From the latter we see that the film is very compliant over about 5 Å just after contact, requiring a force of only ~0.2 μN, and this region gives rise to the contact-area behavior in Figures 2 and 3. The high-compliant region is followed by a broad range from ~0.5 to ~6 μN where the film is virtually noncompliant, and here the friction varies linearly with normal force. Surprisingly, however, an addition compliance covering a measured range of ~3 Å occurs between about 6 and 10 μN, and here the friction again increases in direct proportion to the normal force but at a higher slope. The calculated average applied stress at the 6 μN break point turns out to be ~4 GPa, which is very close to the break stress seen in the direct measurement of friction vs normal force shown in the data of Figure 4.

An average stress at the friction-coefficient break of ~4 GPa is rather high for Au, and one possibility is that the substrate is being plastically deformed or that the SAM films are being physically damaged. However, postmeasurement imaging does not show any evidence of permanent film or substrate damage. This implies that the films are anelastic under these stresses; i.e., some sort of damage is done to the film but it rapidly recovers. As long as this recovery is slow with respect to the friction measurement, energy will be lost and a friction force measured. Earlier calculations of the mechanical compliance of molecular films indicated two such regions of compliance and suggested that the first was the result of the molecules increasing their tilt angle and the second involved a movement of the sulfur headgroup along the surface as a result of the applied force.[32] In the noncomplaint region, the molecules become trapped between the tip and substrate by the interlocking of nested methylene units, which allows them to virtually elastically support large stresses, both compressive and shear, without significant lateral displacement. In separate work aimed at investigating the role of stress in promoting conductance in alkanethiol SAMS on Au surfaces, it was found that conductance through the normally insulating films was only found after the films were significantly stressed.[31] It was concluded from this study that the conductance resulted from stress-induced changes in the electronic structure of the film to achieve closer packing of the compressed molecules. It may be that the internal structures of the alkyl backbones are altered (e.g., from their normally all-trans configuration) to become a more compact molecular solid. In fact, the production of gauche defects with increasing applied stress was found in earlier calculations on SAM films.[33,34]

Concluding Remarks and Perspectives

We have used several examples of recent work applying the IFM to studies of the friction, adhesion, and mechanical properties of self-assembled monolayers of alkanethiol molecules with various combinations of end-group functionality to investigate the relationship between adhesion, friction, and nanomechanical properties. To our knowledge, this is the first time that the intrafilm bonding for an odd methylene-unit −COOH-terminated SAM has been clearly demonstrated. However, this is only the beginning of a systematic investigation of these properties and many combinations remain to be explored. We feel certain that with a continued effort involving a broader range of end-

group combinations and alkyl chain lengths, we will be able to arrive at a reasonably accurate value for the strength of the intrafilm bond for this molecular interaction. One of the major weaknesses of the scanning-probe technique, resulting from its nanoscale look at the world, is the lack of a direct knowledge of the contact area when viewing probe/substrate interactions. This quantity must be determined by suitable contact-mechanics models, and we have demonstrated the use of one longstanding and popular example, i.e., the JKR model. As more applications of modeling using sophisticated molecular-dynamics procedures become available, this problem should become less prohibitive. In conclusion, we hope that the reader will take away at least two impressions from reading this Account: first, the power of scanning probe techniques when used in conjunction with a stable and quantitative force sensor and, second, the critical role that the nanomechanical properties play in determining the adhesive strength of the interfacial interaction and its tribological behavior.

The authors wish to express particular thanks to J. D. Kiely for his untiring efforts in the studies of the nanomechanical properties of Au surfaces. This work was supported by the U.S. Department of Energy under Contract DE-AC04-94AL85000. Sandia is a multiprogram laboratory operated by Sandia Corp., a Lockheed-Martin Co., for the U.S. Department of Energy.

References

(1) Maboudian, R. Surface processes in MEMS technology. *Surf. Sci. Rep.* **1998**, *30*, 207.
(2) Persson, B. N. J. *Sliding Friction*; Springer-Verlag: Berlin, Heidelberg, Germany, 1998.
(3) Heuberger, M.; Luengo, G.; Israelachvili, J. N. Tribology of shearing polymer surfaces. 1. Mica sliding on polymer (PnBMA). *J. Phys. Chem. B* **1999**, *103*, 10127−10135.
(4) Luengo, G.; Campbell, S. E.; Srdanov, V. I.; Wudl, F.; Israelachvili, J. N. Measurement of the adhesion and friction of smooth C-60 surfaces. *Chem. Mater.* **1997**, *9*, 1166−1171.
(5) Israelachvili, J. N.; Chen, Y. L.; Yoshizawa, H. Relationship between Adhesion and Friction Forces. *J. Adhes. Sci. Technol.* **1994**, *8*, 1231−1249.
(6) Berman, A. D.; Ducker, W. A.; Israelachvili, J. N. Origin and characterization of different stick-slip friction mechanisms. *Langmuir* **1996**, *12*, 4559−4563.
(7) Tsukruk, V. V.; Bliznyuk, V. N. Adhesive and friction forces between chemically modified silicon and silicon nitride surfaces. *Langmuir* **1998**, *14*, 446−455.
(8) Noy, A.; Vezenov, D. V.; Lieber, C. M. Chemical force microscopy. *Annu. Rev. Mater. Sci.* **1997**, *27*, 381−421.
(9) Tsukruk, V. V. Molecular lubricants and glues for micro- and nanodevices. *Adv. Mater.* **2001**, *13*, 95−108.
(10) Burnham, N. A.; Colton, R. J. Measuring the Nanomechanical Properties and Surface Forces of Materials Using an Atomic Force Microscope. *J. Vac. Sci. & Technol., A* **1989**, *7*, 2906−2913.
(11) Israelachvili, J. *Intermolecular & Surface Forces*; Academic Press: New York, 1992.
(12) Joyce, S. A.; Houston, J. E. A new force sensor incorporating force-feedback control for interfacial force microscopy. *Rev. Sci. Instrum.* **1991**, *62*, 710−715.
(13) Kiely, J. D.; Houston, J. E. Contact hysteresis and friction of alkanethiol self-assembled monolayers on gold. *Langmuir* **1999**, *15*, 4513.
(14) Kim, H. I.; Boiadjiev, V.; Houston, J. E.; Zhu, X. Y.; Kiely, J. D. Tribological properties of self-assembled monolayers on Au; SiOx and Si surfaces *Tribol. Lett.* **2001**, *10*, 97−101.
(15) Carpick, R. W.; Salmeron, M. Scratching the surface: Fundamental investigations of tribology with atomic force microscopy. *Chem. Rev.* **1997**, *97*, 1163−1194.
(16) Kiely, J. D.; Houston, J. E.; Mulder, J. A.; Hsung, R. P.; Zhu, X. Y. Adhesion, Deformation and Friction for Self-Assembled Monolayers on Au and Si Surfaces. *Tribol. Lett.* **1999**, *7*, 103−107.
(17) Kim, H. I.; Houston, J. E. Separating mechanical and chemical contributions to molecular-level friction. *J. Am. Chem. Soc.* **2000**, *122*, 12045−12046.
(18) Carpick, R. W.; Agrait, N.; Ogletree, D. F.; Salmeron, M. Measurement of interfacial shear (friction) with an ultrahigh vacuum atomic force microscope. *J. Vac. Sci. Technol., B* **1996**, *14*, 1289−1295.
(19) Nuzzo, R. G.; Dubois, L. H.; Allara, D. L. Fundamental-studies of microscopic wetting on organic-surfaces. 1. Formation and structural characterization of a self-consistent series of polyfunctional organic monolayers. *J. Am. Chem. Soc.* **1990**, *112*, 558−569.
(20) Sun, L.; Kepley, L. J.; Crooks, R. M. Molecular-interactions between organized; surface-confined monolayers and vapor-phase probe molecules: hydrogen-bonding interactions. *Langmuir* **1992**, *8*, 2101−2103.
(21) Carpick, R. W.; Agrait, N.; Ogletree, D. F.; Salmeron, M. *J. Vac. Sci. Technol., B* **1996**, *B14*, 1289.
(22) Johnson, K. L.; Kendall, K.; Roberts, A. D. *Proc. R. Soc. London* **1971**, *A324*, 301.
(23) Hertzberg, R. W. *Deformation and Fracture Mechanics of Engineering Materials*, 3rd ed.; John Wiley and Sons: New York, 1989.
(24) Kiely, J. D.; Houston, J. E. Indentation Modulus and Yield Point of Au(111), (001) and (110). *Mater. Res. Soc. Symp. Proc.* **1998**, *522*, 125−131.
(25) Kiely, J. D.; Hwang, R. Q.; Houston, J. E. Effect of Surface Steps on the Plastic Threshold in Nanoindentation. *Phys. Rev. Lett.* **1998**, *81*, 4424−4427.
(26) Kiely, J. D.; Houston, J. E. Nanomechanical Properties of Au(111), Au(001), and Au(110) Surfaces. *Phys. Rev. B* **1998**, *57*, 12588−12594.
(27) Michalske, T. A.; Houston, J. E. Dislocation nucleation at nanoscale mechanical contacts. *Acta Mater.* **1998**, *46*, 391−396.
(28) Leo, A.; Charych, D. H.; Salmeron, M. Comparative atomic force microscopy study of the chain length dependence of frictional properties of alkanethiols on gold and alkylsilanes on mica. *J. Phys. Chem. B* **1997**, *101*, 3800−3805.
(29) McDermott, M. T.; Green, J.-B. D.; Porter, M. D. Scanning force microscopic exploration of the lubrication capabilities of *n*-alkanethiolate monolayers chemisorbed at gold Structural basis of microscopic friction and wear. *Langmuir* **1997**, *13*, 2504−2510.
(30) Xiao, X.; Hu, J.; Charych, D. H.; Salmeron, M. Chain length dependence of the frictional properties of alkylsilane molecules self-assembled on Mica studied by atomic force microscopy. *Langmuir* **1996**, *12*, 235−237.
(31) Son, K. A.; Kim, H. I.; Houston, J. E. Role of stress on charge transfer through self-assembled alkanethiol monolayers on Au. *Phys. Rev. Lett.* **2001**, *86*, 5357−5360.
(32) Tupper, K. J.; Brenner, D. W. Compression-induced structural transition in a self-assembled monolayer. *Langmuir* **1994**, *10*, 2335−2338.
(33) Siepmann, J. I.; McDonald, I. R. Monte Carlo Simulation of the mechanical relaxation of a self-assembled monolayer. *Phys. Rev. Lett.* **1993**, *70*, 453−456.
(34) Mikulski, P. T.; Harrison, J. A. Packing-density effects on the friction of *n*-alkane monolayers. *J. Am. Chem. Soc.* **2001**, *123*, 6873−6881.

AR9801144